Published in IET Power Electronics
Received on 11th September 2013
Revised on 11th January 2014
Accepted on 4th February 2014
doi: 10.1049/iet-pel.2013.0654

ISSN 1755-4535

Hierarchy control of power quality for wind – battery energy storage system

Kai Li[1], *Hongbing Xu*[1], *Qian Ma*[1], *Ji Zhao*[2]

[1]*School of Automation Engineering, University of Electronic Science and Technology of China, Chengdu, People's Republic of China*
[2]*Department of Power Electronics and Control, Dongfang Electric Corporation, Chengdu, People's Republic of China*
E-mail: autolikai@gmail.com

Abstract: Uncertainty of the wind results in a fluctuating power output of wind turbine generators, and consequently, causes adverse impacts on the stability of system frequency and voltage. To smooth such power fluctuation, this study proposes a power quality control strategy based on a three-level hierarchical structure for wind – battery energy storage hybrid power system, including grid demand calculating level, energy management level and voltage-source converters control level. The advantage of the control strategy is that the state of charge of a battery energy storage system is regulated within proper range and the voltage at the point of common coupling is kept stable while smoothing wind power. Effectiveness of the proposed method is validated by MATLAB/SIMULINK simulations and experiments.

1 Introduction

As clean and inexhaustible energy source, wind power industry is developing fast throughout the world in recent years. However, because of the intermittency and uncertainty of wind, power output of wind farms fluctuates. This brings challenges to the existing power system, such as grid interconnection, voltage and frequency regulation, power quality and reliability [1].

An effective solution to improve the reliability and performance of wind power systems is to integrate energy storage devices into power system network. In [2], different feasible electricity storage technologies are compared for their energy costs and efficiencies over different time scales, and key aspects of the use of energy storage are captured by the probabilistic approach. Among those storage devices, large batteries, flywheels, supercapacitors and superconducting magnetic energy storage are identified as promising wind energy storage options [3, 4], their applications in wind power system have been widely studied as in [5–13].

Since a large-scale battery energy storage system (BESS) is rather expensive, a control strategy is necessary for optimal use of the available BESS [8]. Some control method adopted is based on a first order low-pass filter (LPF), which filters the high-frequency fluctuation component in the wind power to obtain a smoother output power [8–11]. Besides that, some modern control methods also have been applied in control strategies to achieve a better control effect. A knowledge-based neural network management algorithm is proposed in [10] and a fuzzy logic control approach using a Kalman filter instead of a LPF is proposed in [12]. In order to keep the charging level of the battery within its proper range while smoothing wind power output fluctuation, a proper control strategy that can effectively smooth power fluctuation under the premise of stabilising the state of charge (SOC) at a reasonable level is necessary. Moreover, the researches above only focused on active power control to suppress the output power fluctuation without taking advantage of the converter in the system to support the grid voltage by reactive power compensation. With this background, a hierarchical structure-based control strategy of a power conditioning system (PCS) with BESS is proposed.

This paper is organised as follows. Section 2 introduces a hybrid power system of wind power and BESS. Section 3 describes the proposed control scheme. Test results are given in Section 4. Section 5 describes the control system performance and conclusion.

2 Hybrid wind power/BESS

Fig. 1 illustrates a scenario of using energy storage devices to help a wind power generation system regulate the power injected to the grid. Storage batteries are connected to the system at the point of common coupling (PCC) through the PCS. The wind farm output is connected to PCC through a wind power converter. The PCS consists of a voltage-source converter (VSC) and its control system. The three-phase four-quadrant VSC can work as a rectifier/inverter to charge/discharge the batteries. Its control system samples the active power of wind power output of a wind farm, P_{wind} and determines the work mode of VSC to smooth the total active power at the PCC. In order to support the voltage at the PCC, the control system also

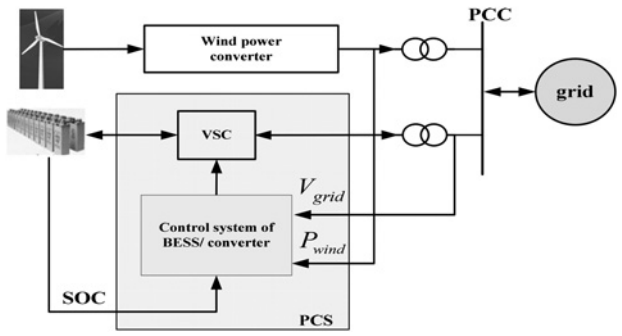

Fig. 1 *Hybrid wind power/BESS*

samples the grid side voltage V_{grid}, and make the VSC absorb or generate reactive power.

3 Hierarchical structure-based power quality control strategy

Fig. 2 shows the hierarchical control strategy of the BESS, which consists of a grid demand calculating level, an energy management level and a VSC control level. The grid demand calculating level includes an active power smoothing module and a reactive power compensation module. To meet the requirement of the rate of change of active power, the active power smoothing module calculates the value of active power P_{ref} which should be generated by BESS. To reduce voltage variation of grid, the reactive power compensation module calculates the reactive power demand Q_{ref}. The energy management level includes a battery energy management module and a reactive energy management module. The battery energy management module modifies P_{ref} to P^*_{ref} according to the SOC of the batteries, so that SOC is kept within a reasonable range while effectively smoothing power fluctuations. The reactive energy management module calculates the maximum reactive power that the VSC can generate or absorb on the basis of current DC and AC voltage, and thus limits the reactive power reference value. VSC control level develops an appropriate control strategy of VSC to track the active power and reactive power reference value.

3.1 Grid demand calculating level

3.1.1 Active power smoothing module: To smooth the power injected into the grid, the real-time output power of wind turbines P_{wind} is sampled and a first order LPF is used to filter out its high-frequency fluctuation component. The filter time constant τ equals to$\left(1/2\pi f_c\right)$, where f_c is the cut-off frequency. Difference between the pre- and post-filtered wind power becomes a target signal for the charging/discharging output of the BESS.

The transfer function of the LPF is given in (1) and the relationship between P_{wind} and P_{ref} is given in (2)

$$G_{filter}(s) = \frac{P_{filter}}{P_{wind}} = \frac{1}{\tau s + 1} \tag{1}$$

$$P_{ref} = \frac{\tau s}{\tau s + 1} P_{wind} \tag{2}$$

where τ is the filter time constant, P_{wind} and P_{filter} are the pre- and post-filtered wind power and P_{ref} is target output of BESS.

3.1.2 Reactive power compensation module: In normal circumstances, fluctuation of utility grid voltage is within ±10% of rated voltage, the VSC still can provide as much reactive power support as possible to lower the fluctuation, as the corresponding reactive power control zone shown in Fig. 3*a*. When grid faults happen and result in voltage sags between 10 and 90% of nominal voltage, VSC should turn into work mode of low voltage ride through (LVRT). LVRT is not discussed in this paper.

As shown in Fig. 3*b*, the reactive power compensation module, receives an input of reference voltage and actual voltage measured at PCC are subtracted so as to activate the operation. A dead zone and a cascade-connected proportional-integral (PI) controller are used to obtain the reference value Q_{ref} for reactive power control. When the voltage deviation ΔV is small (within the dead zone region), the dead zone block generates zero output and Q_{ref} maintains invariant. Parameters tuning of K_{p1} and K_{i1} should consider V/Q static linear droop characteristics and the specific circumstances of voltage and reactive power of wind farms. The control block diagram can also be

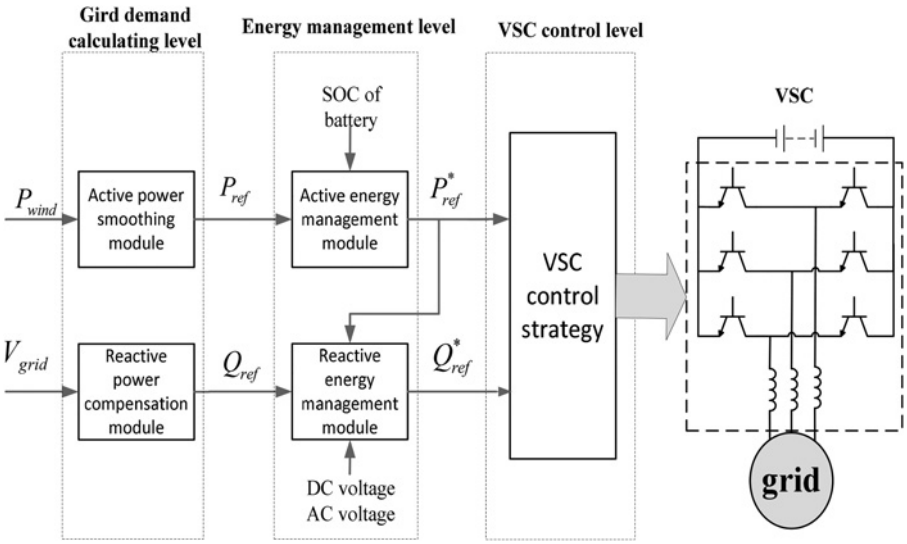

Fig. 2 *Hierarchical structure of the control system*

doi: 10.1049/iet-pel.2013.0654

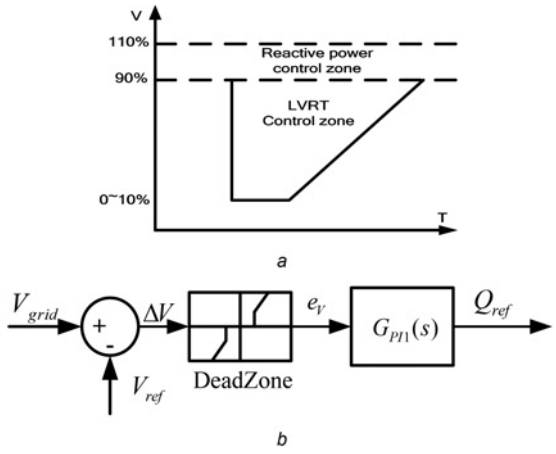

Fig. 3 *Reactive power control*

a Diagram of working region of the reactive power compensation block
b Control block diagram of reactive power

expressed as the following equations

$$\Delta V = V_{\text{grid}} - V_{\text{ref}} \tag{3}$$

$$\begin{cases} e_V = \Delta V, & |\Delta V| \geq c_1 \\ e_V = 0, & |\Delta V| < c_1 \end{cases} \tag{4}$$

$$Q_{\text{ref}} = e_V G_{\text{PI1}} = e_V \left(K_{p1} + \frac{K_{i1}}{s} \right) \tag{5}$$

3.2 Energy management level

3.2.1 Active energy management module: The control block diagram of this management block is shown in Fig. 4. With the real-time feedback of SOC, a PI controller is put after the dead zone block to ensure the SOC of the BESS remains within a proper range which is around the middle point of its capacity. Thus it can avoid the problem of excessive voltage caused by deep charge/discharge cycles. Study on system frequency response in [9, 13] shows that the power systems are sensitive to the medium frequency power fluctuations (between 0.01 and 1 Hz), since the high-frequency power fluctuations are absorbed by generator inertia and the low-frequency ones are damped by the automatic generation control. Therefore the BESS in this paper is designed to suppress fluctuations located in these medium frequency regions. Through a LPF, a low-frequency output below the cut-off frequency is acquired. Then P_{bat} is added to the previous reference value P_{ref} and the output of the active energy management module, that is, the final reference active power of BESS/VSC is obtained. When the difference between SOC_{ref} and the current SOC value SOC_{bat} which can be got from the battery management system is within the dead zone, $P^*_{\text{ref}} = P_{\text{ref}}$, otherwise, $P^*_{\text{ref}} = P_{\text{ref}} + P_{\text{bat}}$. The cut-off frequency of the LPF is better to set to 0.01 Hz or less, to avoid the introduction of the high-frequency component which can weaken fluctuations smoothing effect.

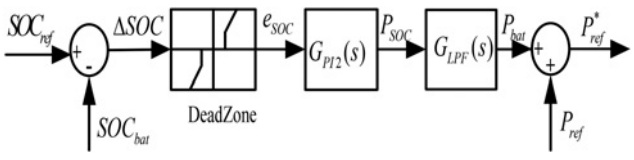

Fig. 4 *Control block diagram of the SOC of the BESS*

The control block diagram can also be expressed as the following equations

$$\Delta\text{SOC} = \text{SOC}_{\text{ref}} - \text{SOC}_{\text{bat}} \tag{6}$$

$$\begin{cases} e_{\text{SOC}} = \Delta\text{SOC}, & |\Delta\text{SOC}| \geq c_2 \\ e_{\text{SOC}} = 0, & |\Delta\text{SOC}| < c_2 \end{cases} \tag{7}$$

$$P_{\text{SOC}} = e_{\text{SOC}} G_{\text{PI2}} = e_{\text{SOC}} \left(K_{p2} + \frac{K_{i2}}{s} \right) \tag{8}$$

$$P_{\text{bat}} = P_{\text{SOC}} G_{\text{LPF}} = P_{\text{SOC}} \frac{1}{\tau_1 s + 1} \tag{9}$$

$$P_{\text{bat}} + P_{\text{ref}} = P^*_{\text{ref}} \tag{10}$$

3.2.2 Reactive energy management module: At a certain DC-link voltage, the maximum amplitude of the AC voltage vector of the three-phase voltage source rectifier (VSR) is determined and the maximum magnitude of the grid voltage vector is also certain, so the working range of the BESS/VSC can be decided, as shown in Fig. 5*a*.

The area on the left side of Fig. 5*a* indicates the operating points VSC can achieve. When the grid voltage fluctuating within 10%, BESS/VSC should provide reactive power support as much as possible, while smoothing fluctuations of wind power output. In Fig. 5, variable $\boldsymbol{U}_{\text{g}}$ represents the amplitude of the three-phase grid voltage vector and variable $\boldsymbol{V}$ represents the amplitude of the three-phase AC voltage vector that the converter generates. The vector $\boldsymbol{V}_{LP}$ is certain if P^*_{ref} has been worked out by the active energy management module, their relationship is expressed in (11).

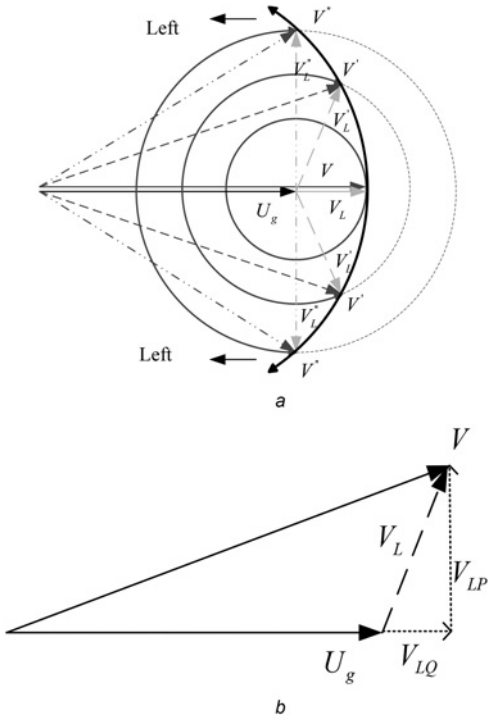

Fig. 5 *Working range of the BESS/VSC*

a Diagram of operating points of VSC
b Vector diagram of operating points of VSC

When adopting the space vector pulse-width modulation algorithm, the maximum amplitude of the three-phase AC voltage vector ($\boldsymbol{V}$) the inverter can generate in the linear pulse-width modulation (PWM) region is $\frac{\sqrt{3}}{3}V_{\mathrm{dc}}$. Thus, (13) can be obtained from Fig. 5*b*

$$\boldsymbol{V}_{LP} = \omega L \frac{P^*_{\mathrm{ref}}}{\boldsymbol{U}_{\mathrm{g}}} \tag{11}$$

$$V_{\max} = \frac{\sqrt{3}}{3} V_{\mathrm{dc}} \tag{12}$$

$$V_{LQ} = \sqrt{V^2 - V_{LP}^2} - \boldsymbol{U}_{\mathrm{g}} \leq \sqrt{\left(\frac{\sqrt{3}}{3}V_{\mathrm{dc}}\right)^2 - V_{LP}^2} - \boldsymbol{U}_{\mathrm{g}} \tag{13}$$

Then, the upper limit of reactive power can be obtained, as shown in the following equation

$$Q \leq \frac{\sqrt{\left(\frac{\sqrt{3}}{3}V_{\mathrm{dc}}\right)^2 - V_{LP}^2} - \boldsymbol{U}_{\mathrm{g}}}{\omega L} \times \boldsymbol{U}_{\mathrm{g}} \tag{14}$$

where Q is the three-phase reactive power.

3.3 VSC control level

VSC control level makes the converter have a fast response to the active and reactive power command calculated by the upper level, and achieves protection of the inverter as well.

In the conventional control strategy of three-phase VSC, rectification and inversion respectively use different control methods. When switching between this two operating modes, the conventional control strategy involves mode hopping and switch of many state variables, there often exists many problems such as unsmooth switching, complex algorithms and slow response. In order to overcome the deficiencies mentioned above, this paper proposes a VSC control strategy to realise unified control of rectification and inversion, and to achieve a smooth handover.

3.3.1 Control strategy: As shown in Fig. 6, the VSC reactive power control adopts the traditional double closed-loop structure and the active power control uses three-loop control structure: AC current inner loop, DC current middle loop and DC voltage outer loop. The set of active power is implemented by way of limitation.

The control strategy unifies the rectification and inversion process in one control block diagram, so the program is convenient to implementation by one control function. The control strategy distinguishes rectification from inversion according to the polarity of active power command. The three-phase reference power P^*_{ref} in this control strategy is used as limiting parameters.

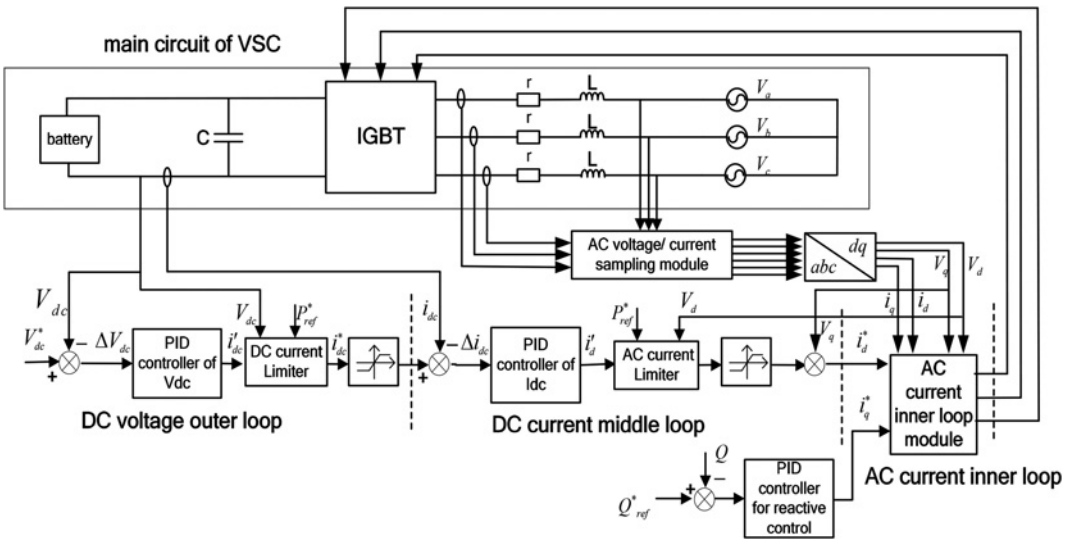

Fig. 6 *Unified control strategy of VSC*

Table 1 Limit of the limiter block

Control loop	Limiter	Static limit		Dynamic limit	
		Upper limit	Lower limit	Border 1	Border 2
DC voltage outer loop	DC current limiter	maximum charging current	maximum discharging current	0	$\frac{P^*_{\mathrm{ref}}}{V_{\mathrm{dc}}}$
DC current middle loop	AC current limiter	maximum active current of rectification	maximum active current of inversion	0	$\frac{P^*_{\mathrm{ref}}}{V_d}$

Notes: (1) Output range of this limiter block is the smaller of static limit and dynamic limit.
(2) The conversion efficiency of the inverter is assumed to be 100%.
(3) AC current limiter is for the *d*-axis current.

doi: 10.1049/iet-pel.2013.0654

The DC voltage outer loop is designed to implement constant voltage charging or discharging of the battery. The reference voltage for this loop is the maximum charging voltage of the battery when in rectification and minimum discharging voltage when in inversion.

Strategy of the DC current limiter module and AC current limiter module in Fig. 6 is illustrated in Table 1, here V_d is the d-axis component of three-phase grid voltage vector on a dq rotating reference frame by using the Park transformation. The static limit is used to ensure safety operation of the battery and VSC and the dynamic limit is used to ensure that the output power follows the track of P^*_{ref}.

3.3.2 Analysis of operating mode: Two typical states of the battery are described in this section, as an example to illustrate the unified control strategy.

Fig. 7*a* is a curve of active power given instructions. ①–⑫ represents 12 different operation points.

The positive and negative values of DC current represent two different modes of work, positive current means rectification and negative current means inversion. When the system is put into operation, the maximum battery charging current, the maximum discharging current, the charge cut-off voltage and the discharge cut-off voltage are determined by the characteristics of the storage batteries. These four parameters, together with the real-time changing given value of active power, thus define the work area of VSC.

Fig. 7*b* shows the trajectories of the operating point. ① presents a standby state. After receiving a given power P1, VSC increases the active power to P1 with rectification mode. The terminal voltage of the battery slowly rises while charging and then the operating point changes to ③. Output power increases to P2 and the operating point changes to ④ when new power instruction P2 is received. VSC runs with constant power P2 until it reaches the operating point ⑤. At this time new power instruction P3 is received, VSC reduces power to P3 and the operating point becomes ⑥. VSC runs with constant power P3 until it reaches the operating point ⑦. If negative given power P4 is received at this time, for the limit of maximum battery discharging current, VSC cannot achieve the set power and will discharge with constant current, meanwhile, the terminal voltage of the battery slowly drops until it reaches the operating point ⑨. After receiving a new given power P5, VSC discharges with constant power P5 until it reaches the operating point ⑫. At last, VSC receives standby command, set the output power to zero and the operating point switches to ⑫.

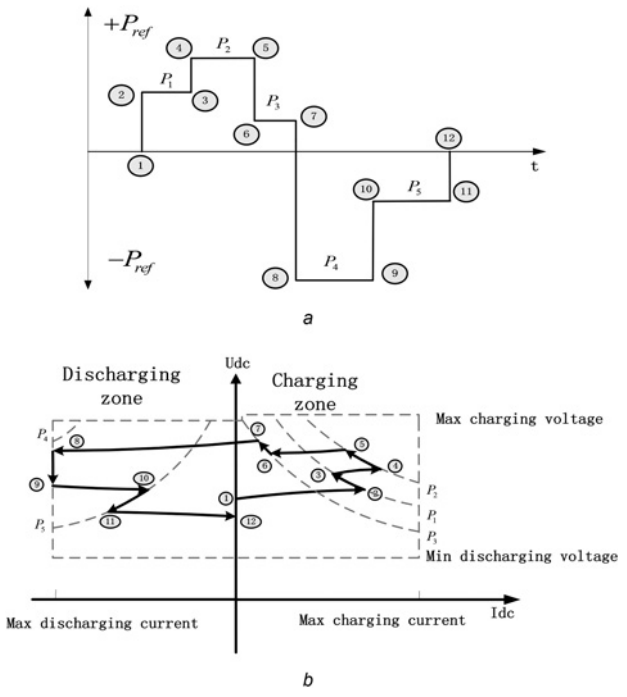

Fig. 7 *Operating mode analysis*

a Curve of given power
b Diagram of the trajectories of the operating point

4 Simulation and experiment results

4.1 Simulation results

A BESS and a PCS model are built in MATLAB to simulate the effectiveness of the control strategy proposed in this paper. The circuit parameters of the simulation and experimental platform are given in Table 2. Other key parameters used in the control strategy is given as follows: $\tau = 15.9$ s, $c_1 = 0.02$, $K_{p1} = 1$, $K_{i1} = 1$, $c_2 = 0.2$, $K_{p2} = 2500$, $K_{i2} = 10$, $\tau_1 = 15.9$ s, $\text{SOC}_{\text{ref}} = 50\%$. The filter time constant τ and τ_1 is set to 15.9 s for the cut-off frequency is set to 0.01 Hz to avoid the introduction of the medium frequency power fluctuations as discussed before in chapter III, parameter c_1 of reactive power compensation module is set to 0.02 to maintain voltage at PCC within 0.98–1.02 of the rated value and parameter c_2 of active energy management module is set to 0.2 to keep SOC of the BESS within 30–70%.

The 1500 s wind power curve used for simulation is from the measured output power curve of single 1.5 MW wind turbine, as shown in Fig. 8*a*. Fig. 8*b* displays the wind power fluctuation spectrum which is got from the fast Fourier transform.

Fig. 8*c* shows the comparison of pre- and post-filtered wind power and Fig. 8*d* displays the fluctuation spectrum of filtered wind power.

Fig. 9*a* shows the curve of reference power for BESS which is the difference between the pre-filtered power and the post-filtered power, and the other curve is the actual response curve in the simulation. Fig. 9*b* shows the 300 s zoom of Fig. 9*a*.

Comparison diagram of battery SOC in case of with and without SOC feedback control is displayed in Fig. 9*c*. In the simulation, the initial SOC of the battery is 50 and 30–70% is chosen as the range of the dead zone in the battery energy management block. At 500 s, SOC reaches the lower limit 30% and the battery energy management

Table 2 Parameter of three-phase grid-connected convertor

System parameters	Values
rated active power	simulation: 400 kW experiment: 100 kW
switching frequency	9 kHz
line voltage of grid root mean square	380 V
DC voltage range	300–600 V
ratio of the three-phase transformer installed inside PCS	1.4:1
inductance on the invertor side	1.2 mH
inductance on the grid side	0.9 mH
capacitor of the inductor-capacitor-inductor (LCL) filter	10.5 μF
resonant frequency of the LCL filter	2.17 kHz

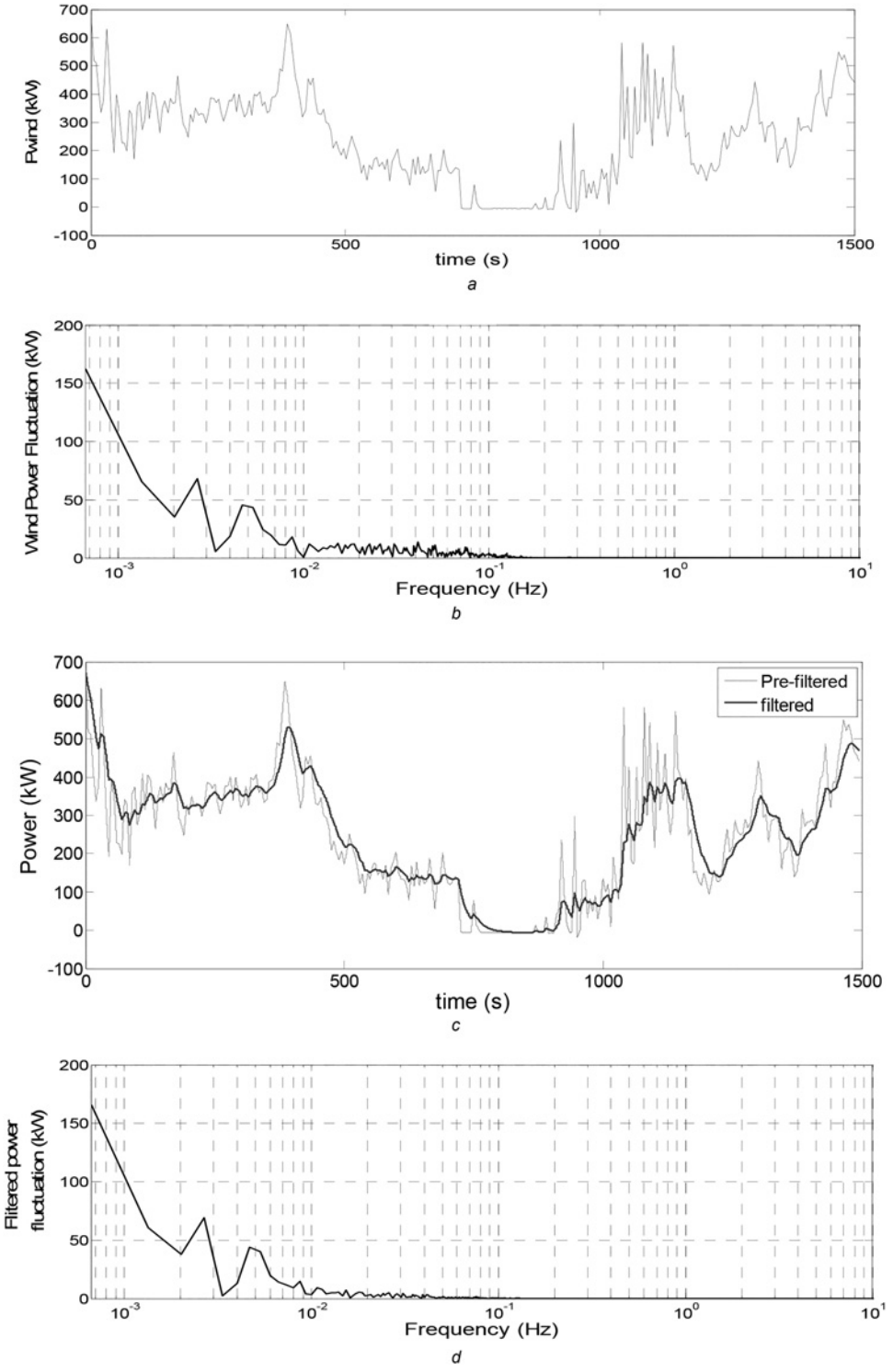

Fig. 8 *Wind power and frequency analysis*

a Original power output of single wind turbine
b Its power fluctuation spectrum
c Pre- and post-filtered wind power
d Frequency spectrum of post-filtered wind power.

block begins working and trying to regulate SOC back to proper range. From 500 to 900 s, the SOC curve with SOC control is above the one without SOC control. At about 900 s, SOC of the curve with SOC control returns to 30% whereas the other one is 21%, that is lower than the set limit.

In order to quantitatively evaluate the power fluctuations over particular frequency regions, the fluctuation harmonic content (FHC) in the frequency domain is introduced as in [11]

$$\mathrm{FHC}\,(F) = \frac{\sqrt{\sum_{f\in\{F\}} \left(P(f)/\sqrt{2}\right)^2}}{P_0} \tag{15}$$

Here F is the frequency region and P_0 is the DC component or the average power.

doi: 10.1049/iet-pel.2013.0654

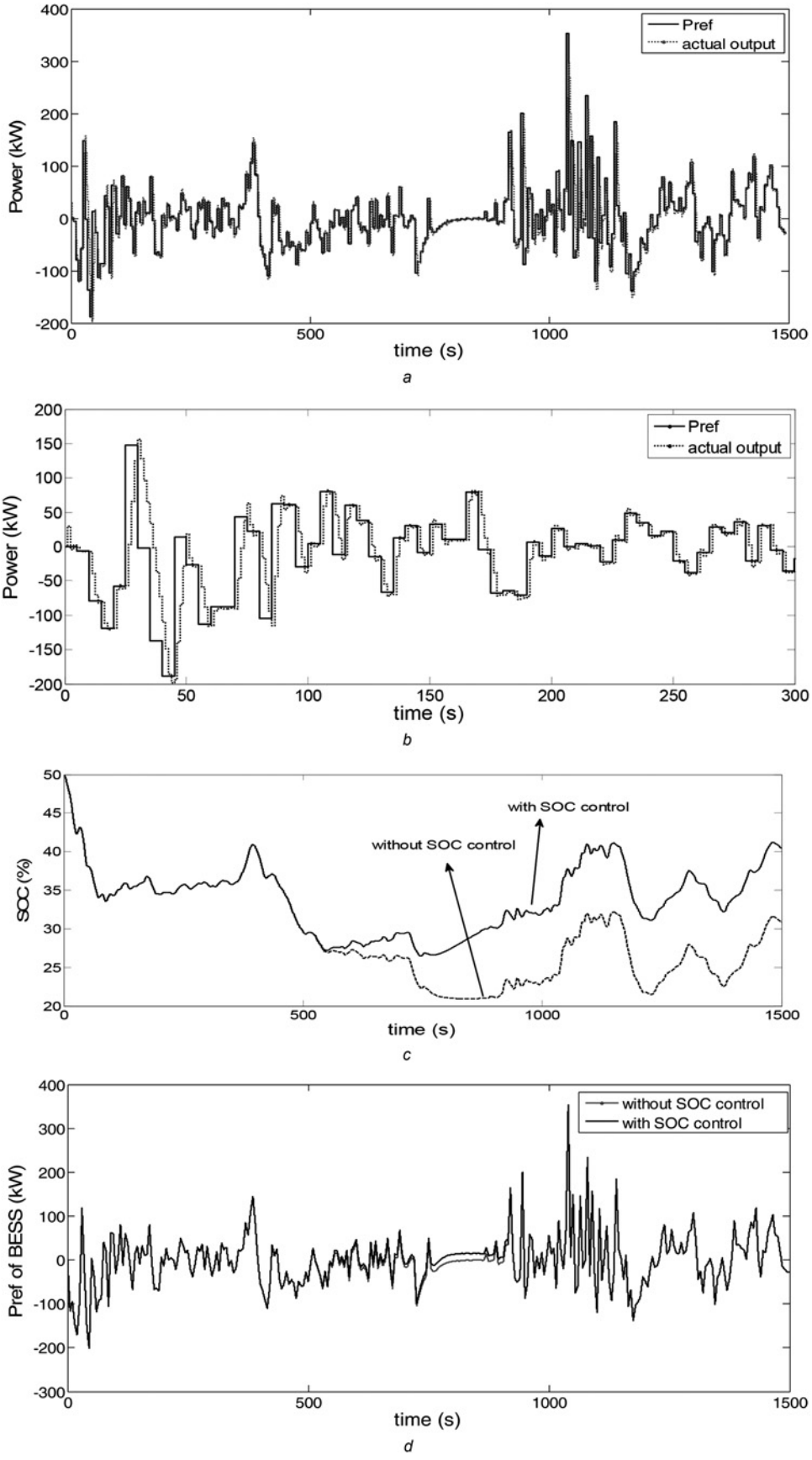

Fig. 9 *Simulation results*

a Reference power for BESS and the actual response curve
b Zoom of reference power curve and actual response curve of BESS
c Diagram of SOC with and without SOC feedback control
d Comparison diagram of reference power for BESS with and without SOC control

Table 3 FHC values of wind powers in simulations

Frequency region	Low (<0.01 Hz)	Medium (0.01~1 Hz)	High (>1 Hz)	Full region
pre-filtered P_{wind}, %	29.86	10.60	0.28	31.68
filtered P_{wind} without energy management of batteries, %	29.49	4.03	0.24	29.77
filtered P_{wind} with energy management of batteries, %	30.54	4.09	0.24	30.81

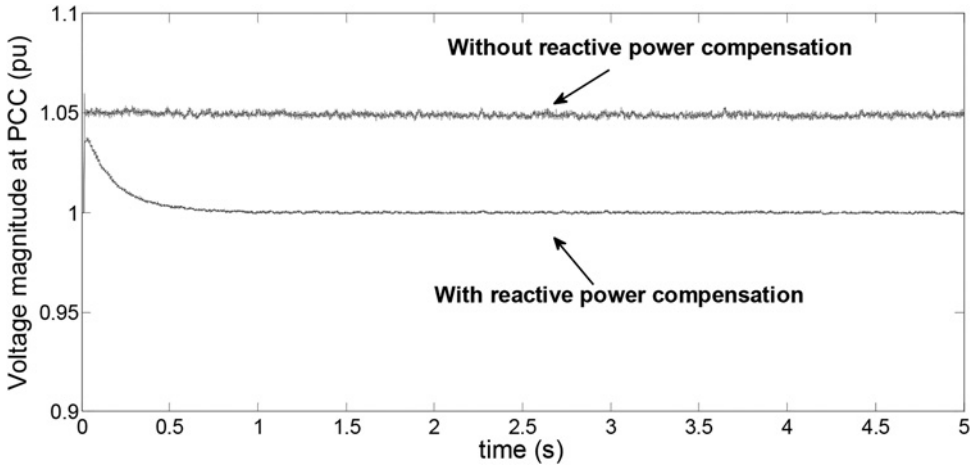

Fig. 10 *Voltage magnitude at PCC with and without reactive power compensation*

For clear comparison, the FHC values of different cases are calculated and tabulated in Table 3. In the targeted 0.01~1 Hz frequency region, fluctuations reduce significantly both in the filtered power with SOC control and without SOC control.

Fig. 10 shows the voltage magnitude at the PCC in the case of a constant current reference. The upper curve represents the uncompensated voltage at PCC whereas the lower one represents the voltage with reactive power compensation. Evidently, the voltage at the PCC is maintained at 1 pu with reactive power compensated by VSC/BESS.

4.2 Experimental results

A 100 kW prototype of energy storage VSC is designed and implemented for verifying the theoretical analysis, its parameters is listed in Table 2 and the experimental platform is displayed in Fig. 11.

Fig. 12*a* shows the actual output curve of convertor when a curve in Fig. 7*a* is given as power reference. P1–P5 are 30, 40, 15, −45 and −20 kW, respectively. In this experiment, the maximum battery discharging current value is set to −80 A (negative means inversion as mentioned before). When VSC receives the −45 kW command, its output power and current keep increasing until the DC current reaches the limit of −80 A, then BESS discharges with this constant current and the output power maintains at about −40 kW which is lower than the set power. Fig. 12*b* shows the 1500 s actual output power curve. Fig. 12*b* is obtained by adopting the required power curve for BESS in Fig. 8*c* as the power reference. Note that the actual output power is limited within ±100 kW because of the output capacity limit of VSC. Besides that, VSC is capable of trace the given instruction fast and accurately. Fig. 12*c* displays the experimental curve of battery SOC in case of with and without SOC feedback control. In order to clearly test the SOC control effect with a battery of 180 AH, the lower

Fig. 11 *Experimental platform of VSC and the wind farm for experiments*

limit of dead zone is set to 0.448, that is, parameter c_2 of active energy management module is set to 0.012, which is smaller than the one used in simulations. Evidently, SOC is well regulated with the help of SOC feedback control.

From the data obtained in experiments, FHC values are calculated and tabulated in Table 4 for analysis. By comparison, the experimental result is in agreement with the simulation results, except that fluctuation in the targeted medium frequency region is slightly greater, and this is caused by the capacity limit of VSC adopted in experiments.

5 Conclusions

In this paper, a control system for BESS/VSC is designed based on three-level hierarchical control. The primary control level is the grid demand calculating level which

doi: 10.1049/iet-pel.2013.0654

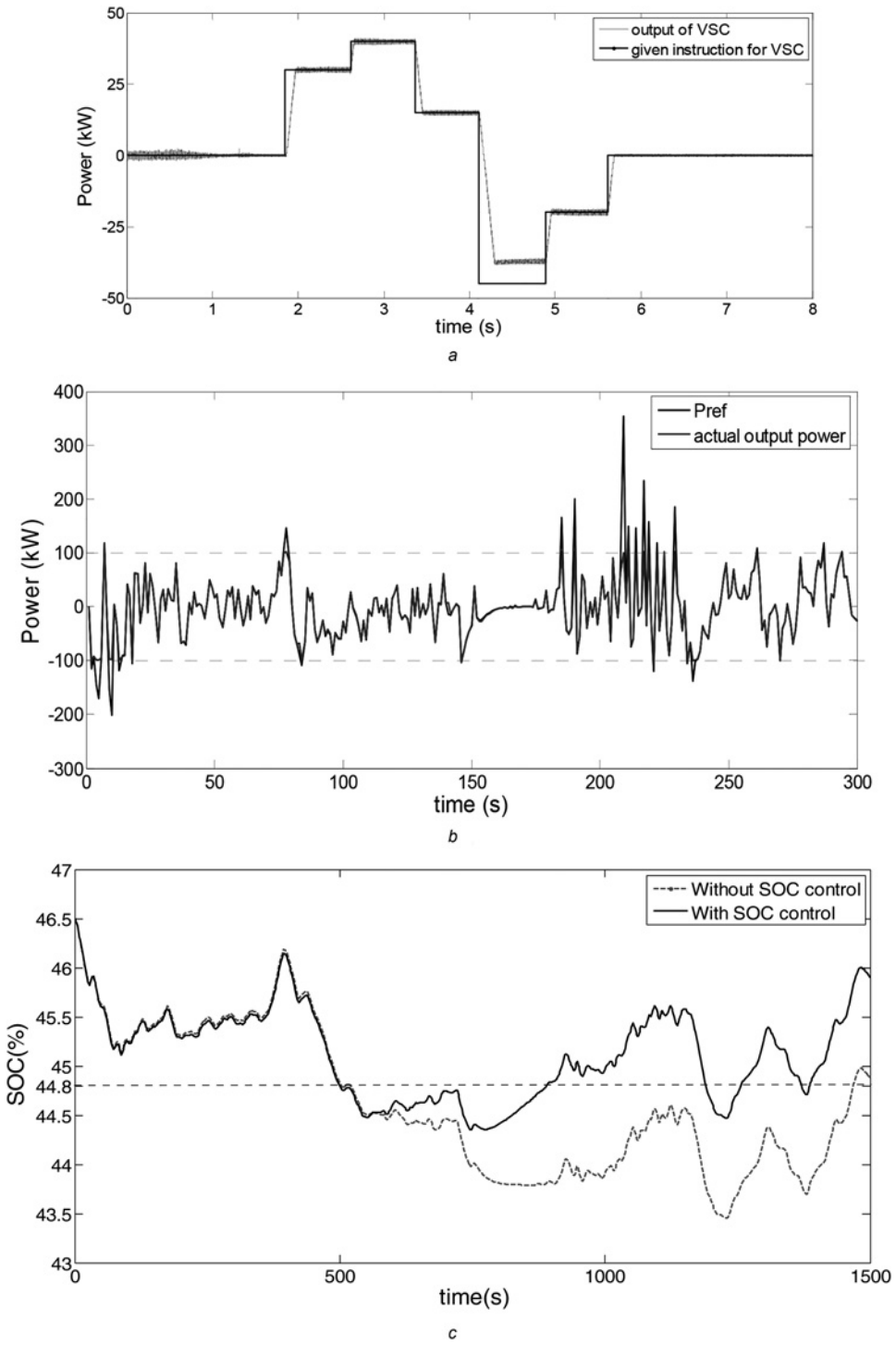

Fig. 12 *Experimental results*

a Response curve of different operation points
b Comparison diagram of reference power and actual output
c Comparison diagram of SOC with and without SOC feedback control

Table 4 FHC values of wind powers in experiments

Frequency region	Low (<0.01 Hz)	Medium (0.01~1 Hz)	High (>1 Hz)	Full region
pre-filtered P_{wind}, %	29.86	10.60	0.28	31.68
filtered P_{wind} without energy management of batteries, %	28.98	5.51	0.24	29.50
filtered P_{wind} with energy management of batteries, %	30.02	5.61	0.24	30.54

processes the grid demand. The secondary control level is energy management level and it calculates the output capability of active and reactive power according to present state of the batteries and converters. And the third control

level is the VSC control level which ensures that the BESS power output matches the instruction given by the secondary control level. Both the simulation model and the experiment platform are set up and the results are summarised as follows:

1. The smoothing effect of the BESS is significant without considering the SOC control. Fluctuation in the full frequency range is reduced by 1.91%. In the target medium frequency range, the fluctuation is reduced by 6.57% and decrease to 38% of its original value.
2. With the injection of reactive power, the voltage at the PCC is successfully kept at 1.0 pu.
3. Thanks to the SOC feedback control introduced in the battery energy management block, battery SOC is effectively regulated within proper range.
4. When the battery SOC is taken into account, the output fluctuation in the medium frequency range increases to 4.09%, which is 1.015 times of the value without SOC control. Therefore the fluctuation smoothing performance of the system is not much affected.

6 References

1 Teleke, S., Baran, M.E., Huang, A.Q., Bhattacharya, S., Anderson, L.: 'Control strategies for battery energy storage for wind farm dispatching', *IEEE Trans. Energy Convers.*, 2009, **24**, (3), pp. 725–732

2 Barton, J.P., Infield, D.G.: 'Energy storage and its use with intermittent renewable energy', *IEEE Trans. Energy Convers.* ,2004, **19**, (2), pp. 441–448

3 Guerrero, M.A., Romero, E., Barrero, F., Milanés, M.I., González, E.: 'Overview of medium scale energy storage systems'. Compatibility and Power Electronics Conf., May 2009, pp. 93–100

4 Spahic, E., Balzer, G., Hellmich, B., Munch, W.: 'Wind energy storages-possibilities'. Power Tech Conf., Lausanne, July 2007, pp. 615–620

5 Abbey, C., Joos, G.: 'Supercapacitor energy storage for wind energy applications', *IEEE Trans. Ind. Appl.*, 2007, **43**, (3), pp. 769–776

6 Saejia, M., Ngamroo, I.: 'Alleviation of power fluctuation in interconnected power systems with wind farm by SMES with optimal coil size', *IEEE Trans. Appl. Supercond.*, 2012, **22**, (3), pp. 5701504–5701504

7 Suvire, G.O., Molina, M.G., Mercado, P.E.: 'Improving the integration of wind power generation into AC microgrids using flywheel energy storage', *IEEE Trans. Smart Grid*, 2012, **3**, (4), pp. 1945–1954

8 Yoshimoto, K., Nanahara, T., Koshimizu, G.: 'New control method for regulating state-of-charge of a battery in hybrid wind power/battery energy storage system'. IEEE PES Power Systems Conf. and Exposition, October 2006, pp. 1244–1251

9 Li, W., Joos, G., Abbey, C.: 'Wind power impact on system frequency deviation and an ESS based power filtering algorithm solution'. IEEE PES Power Systems Conf. and Exposition, October 2006, pp. 2077–2084

10 Abbey, C., Strunz, K., Joós, G.: 'A knowledge-based approach for control of two-level energy storage for wind energy systems', *IEEE Trans. Energy Convers.*, 2009, **24**, (2), pp. 539–547

11 Li, W., Joós, G.: 'Comparison of energy storage system technologies and configurations in a wind farm'. Power Electronics Specialists Conf., June 2007, pp. 1280–1285

12 Li, X.: 'Fuzzy adaptive Kalman filter for wind power output smoothing with battery energy storage system', *IET Renew. Power Gener.*, 2012, **6**, (5), pp. 340–347

13 Luo, C., Ooi, B.T.: 'Frequency deviation of thermal power plants due to wind farms', *IEEE Trans. Energy Convers.*, 2006, **21**, (3), pp. 708–716

doi: 10.1049/iet-pel.2013.0654